Journal of Astronomical Telescopes, Instruments, and Systems

AstronomicalTelescopes.SPIEDigitalLibrary.org

Semianalytical error budget for adaptive optics systems with pyramid wavefront sensors

Guido Agapito
Enrico Pinna

SPIE.

Guido Agapito, Enrico Pinna, "Semianalytical error budget for adaptive optics systems with pyramid wavefront sensors," *J. Astron. Telesc. Instrum. Syst.* **5**(4), 049001 (2019), doi: 10.1117/1.JATIS.5.4.049001.

Semianalytical error budget for adaptive optics systems with pyramid wavefront sensors

Guido Agapito* **and Enrico Pinna**
Osservatorio Astrofisico di Arcetri, Firenze, Italy

Abstract. We present the error budget of an astronomical single conjugated adaptive optics system with a pyramid wavefront sensor. The chosen approach is semianalytical to take into account the full response characteristics of this kind of sensor, and, in addition to these characteristics, it includes the closed-loop dynamics and all the main error sources: fitting, temporal, measurement, and aliasing error. This error budget has been made to complement more complex numerical simulators in the system design process, to rapidly explore a huge range of system parameters and to assess the critical components. Its reliability is demonstrated with a comparison with Monte Carlo numerical simulations on a reference system, the Single Conjugated Adaptive Optics Upgrade for Large Binocular Telescope. [DOI: 10.1117/1.JATIS.5.4.049001]

Keywords: adaptive optics; wavefront sensors; simulations; astronomy; telescopes.

Paper 19046 received May 3, 2019; accepted for publication Sep. 16, 2019; published online Oct. 10, 2019.

1 Introduction

Adaptive optics (AO) is becoming a key feature of large ground-based telescopes at optical/near-infrared wavelengths, allowing recovery of the diffraction limit of such large apertures. Most of the 8/10-m class of telescopes is equipped with AO,[1–5] and the next generation of extremely large telescopes will have several AO-equipped instruments.[6–12] On the other hand, AO system complexity is increasing because of the telescope size and the tighter goals required by new instrumentation. Hence, AO system design is becoming more complex and critical.

In this context, an AO error budget software is a key tool: exploring the different system parameters (number of actuators, sampling frequency, number of subapertures, etc.) with an end-to-end simulator is time-consuming, and it does not allow easy identification of the different error terms. Instead, an error budget software allows to explore huge range of system parameters, providing the error term distribution that is essential in the system design phase.

In the literature, we find several error budget tools—such as the Shack–Hartmann (SH) wavefront sensor (WFS) analytical model presented by Rigaut et al.,[13] PAOLA,[14,15] and others[16–20]—nowadays, are routinely employed for the AO system design. However, until recently,[20] no analytical model was able to describe the pyramid wavefront sensor (P-WFS) in partial correction regime. Such a sensor, working with the full-aperture point spread function, changes its sensitivity in partial correction conditions.[21] Here we report our work, started in 2016 for the Single Conjugated Adaptive Optics Upgrade for Large Binocular Telescope (LBT) (SOUL) system design,[22] in which we developed an error budget tool that is capable of dealing with P-WFS. We introduced two main items with respect to what is available in the literature. The first one is a numerical component, taking into account the response characteristics of the P-WFS, following the same approach proposed by Fusco et al.[23] for the case of the SH WFS. The second one is the adoption of a modal control[24] like the real system: a tool that deals with the same control architecture of the real system is a useful feature that can be used to optimize specific control parameters as it is shown in this work and by Agapito et al.[25]

In this work we describe such a semianalytical tool emulating a single conjugate AO (SCAO) system, composed of a P-WFS, deformable mirror (DM), and a real-time computer (RTC). The architecture of this system is depicted in Fig. 1. Note that our tool could be used as a component to model more complex AO systems, such as ground layer and multiconjugate adaptive optics (MCAO) systems.

The paper will continue in the next section with a description of the algorithms: in Sec. 2.1, we will introduce the transfer functions (TFs) of the closed loop that will be used to compute some of the error terms, and all the error terms are presented in Sec. 2.2. Then, we show how the error budget can be used to optimize an AO system and we present the results of the optimization of SOUL[22] in Sec. 3, and, finally, in Sec. 4, we report a comparison with end-to-end simulation.

2 Error Budget Machine

The algorithm, hereafter "the machine," provides the estimation of the residual wavefront (WF) error for each of its components (Sec. 2.2) for a given system configuration (Sec. 4). These residuals are analytically computed, due to the closed-loop transfer functions (CLTFs) (as in PAOLA[14]) where we introduced some elements obtained via end-to-end numerical simulation: we are referring to the WFS's TF, reconstruction matrix, and aliasing. The first one, in the case of the P-WFS, is highly dependent on the WF residuals. This semianalytical approach allows having an effective error budget algorithm for AO system adopting the pyramid as WFS. In this section, we will detail, as first (Sec. 2.1), the considered TFs and then (Sec. 2.2) the error terms.

2.1 *Closed-Loop Transfer Functions*

Below, we briefly describe the CLTFs. They model the response between two points of the closed loop, and they can be used to

*Address all correspondence to Guido Agapito, E-mail: guido.agapito@inaf.it

2329-4124/2019/$28.00

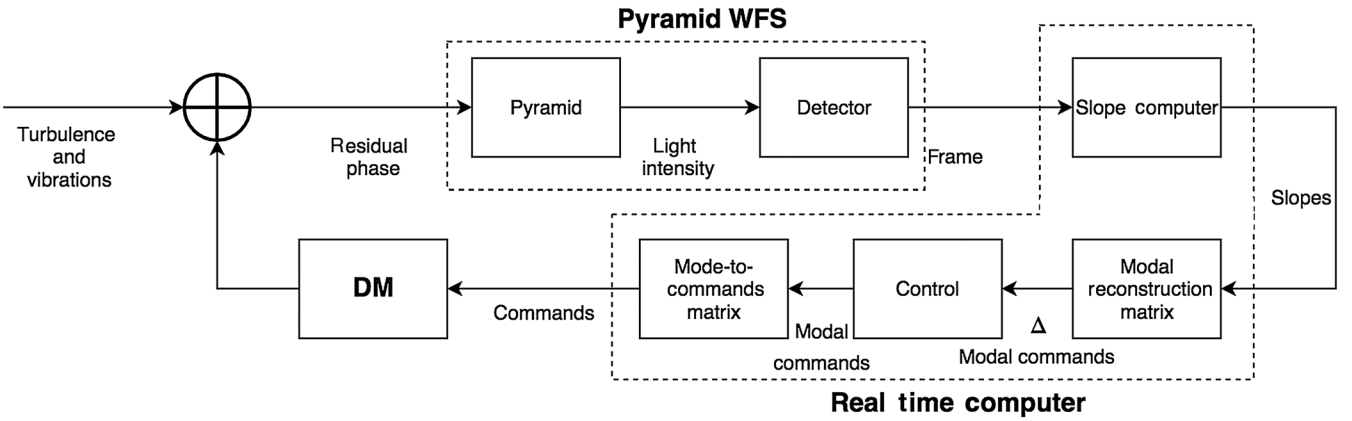

Fig. 1 Schematic representation of the considered SCAO system architecture. The principal devices characterizing the control loop are P-WFS, DM, RTC, which comprise the reconstruction matrix, the control, and the modes-to-commands matrix. We use a modal representation of the WF, and thus a modal control (see Sec. 5.2.1 of Beckers[24]), because it gives us the ability to decouple most of the error terms on an orthogonal modal base.

compute the effect of the closed loop on the temporal power spectral density (PSD) of an input signal x as

$$\mathrm{PSD}\{y\} = |H(\omega)|^2 \mathrm{PSD}\{x\}, \tag{1}$$

where y is the output signal, $H(\omega)$ is the CLTF, and the operator

$$\mathrm{PSD}\{x\} \triangleq \langle |\hat{x}(\omega)|^2 \rangle \tag{2}$$

denotes the temporal PSD of x, and $\hat{x}(\omega)$ is the Fourier transform of the signal x.

Considering that

$$\sigma_y^2 = \int \mathrm{PSD}\{y\} \mathrm{d}\omega = \int |H(\omega)|^2 \mathrm{PSD}\{x\} \mathrm{d}\omega, \tag{3}$$

we will use two of these CLTFs to compute the error terms in the next sections. These CLTFs are:

- the rejection transfer function (RTF), H_r, that is the TF between WF disturbances (turbulence and vibrations) and the residual phase and
- the noise transfer function (NTF), H_n, that is the TF between measurement noise and the residual phase.

As mentioned in Sec. 1, we follow a modal control approach; we express the WF by a linear combination of orthogonal Karhunen–Loéve modes.[26] So, considering the decomposition on such modal base, we can define the RTF for the i'th mode as

$$H_r^i(\omega) = \frac{1}{1 + W^i(\omega) R^i(\omega) M^i(\omega) C^i(\omega)}, \tag{4}$$

and the NTF as

$$H_n^i(\omega) = \frac{R^i(\omega) M^i(\omega) C^i(\omega)}{1 + W^i(\omega) R^i(\omega) M^i(\omega) C^i(\omega)}, \tag{5}$$

where

- $W^i(\omega) = \rho^i d(T_{\mathrm{WFS}})$ is the WFS TF of the i'th mode.
- $R^i(\omega) = d(T_{\mathrm{RTC}})$ is the RTC TF of the i'th mode.
- $M^i(\omega) = d(T_{\mathrm{ASM}})$ is the adaptive secondary mirror (ASM) TF of the i'th mode.
- $C^i(\omega)$ is the integrator controller TF of the i'th mode with gain g^i.
- ρ^i is the WFS sensitivity loss factor for the i'th mode.
- $d(x)$ is the delay TF of a time x.
- T_{WFS} is the delay given by the WFS.
- T_{RTC} is the delay given by the RTC.
- T_{ASM} is the delay given by the ASM.

Note that we have introduced the factor ρ^i in the WFS TF to take into account the pyramid loss in sensitivity due to the AO partial correction regime. This factor ρ^i measures the ratio between the WFS sensitivity stored in the interaction matrix (IM) and the actual one during system operation. The two sensitivities differ because the IM is generally acquired in diffraction-limited conditions (in a controlled environment or in a numerically simulated system with a negligible uncorrected residual), whereas, during operation, the turbulence residual decreases the sensitivity.[21,27–30] The values of ρ^i are estimated by end-to-end simulations, following the modulation/demodulation method presented by Esposito et al.[28]

2.2 *Error Terms*

In this work, we take as example a natural guide star SCAO system. We will not consider terms typical of other kind of AO systems such as the cone effect for the laser guide star or tomographic one for MCAO systems. We consider the total AO error divided into:

- Fitting error σ_{fit}^2,
- Temporal error σ_{temp}^2,
- Measurement noise error $\sigma_{\mathrm{noise}}^2$,
- Aliasing error $\sigma_{\mathrm{alias}}^2$

and so the total error is given as

$$\sigma_{\mathrm{total}}^2 = \sigma_{\mathrm{fit}}^2 + \sigma_{\mathrm{temp}}^2 + \sigma_{\mathrm{noise}}^2 + \sigma_{\mathrm{alias}}^2. \tag{6}$$

Temporal, measurement noise, and aliasing errors are propagated through the AO closed loop and so we must take into account of the temporal TF of the system. Instead, fitting error does not depend on the closed-loop behavior of the AO system.

Note that other error terms such as the noncommon path aberrations and anisoplanatic error can affect the total error of a scientific instrument, but in this work they are not taken into account (analytical expressions for anisoplanatic error can be found in Fried[31] and in Roddier[32]).

2.2.1 *Fitting error*

The finite resolution of the WF corrector (the DM) leads to a residual known as fitting error. This residual is generally considered proportional[24] to $(r_E/r_0)^{5/3}$ (where r_E is the DM element size). In this work, since we will considered voice-coil secondary DMs with a Karhunen–Loève basis,[32,33] we will use the formula computed for the LBT-ASM by Quirós-Pacheco et al.:[34]

$$\sigma^2_{\text{fit}} = 0.2778\ N^{-0.9}\left(\frac{D}{r_0}\right)^{\frac{5}{3}}, \tag{7}$$

where N is the mode number, D is the telescope diameter, and r_0 is the Fried's parameter.

2.2.2 *Temporal error*

The temporal error is the residual AO error given by the evolution of the turbulent incoming WF and of the telescope structure vibrations. In this work, we consider its modal representation:

$$\sigma^2_{\text{temp}} = \sum_i \int |H^i_r(\omega)|^2(\text{PSD}\{a^i_{\text{tur}}\} + \text{PSD}\{a^i_{\text{vib}}\})\text{d}\omega, \tag{8}$$

where H^i_r is the RTF, a^i_{tur} is the atmospheric turbulence, a^i_{vib} is the vibration, and the superscript i still indicates the contribution on the i'th mode of the considered basis. Note that we considered the PSDs of the Karhunen-Loève basis coefficients equivalent to Zernike coefficients. These spectra are characterized by an asymptotic $f^{-17/3}$ law for frequencies $>f_c$ and a flat f^0 law for $f < f_c$ (multilayer turbulence profile). The cut-off frequency, f_c, is given as

$$f_c(n^i) \simeq 0.3(n^i + 1)\frac{V}{D}, \tag{9}$$

and n^i is the radial order of the i'th Zernike/Karhunen–Loève, D is the telescope diameter, and V the median wind speed.[35] The integral of each modal PSD is set to match the variance of the Von-Karman turbulence model with the specified r_0 and L_0 values.

2.2.3 *Measurement noise error*

The measurement made by the system WFS is always affected by noise. The sources of noise are the photon propagation and the detector (read-out and dark current). The noise is propagated from the detector pixels to each modal residual in three steps:

- from detector pixels to slopes (slope computation);
- from slopes to modal differential commands (modal reconstruction); and
- from modal differential commands to modal residual (CLTF).

The modal representation of the so-called measurement noise error term is given as

$$\sigma^2_{\text{noise}} = \sum_i \int |H^i_n(\omega)|^2\text{PSD}\{w^i\}\text{d}\omega, \tag{10}$$

where $H^i_n(\omega)$ is the NTF and w^i is the measurement noise propagated on the modes. This noise w^i has a flat temporal PSD, and so it is fully characterized by its spectrum level or its variance:

$$\sigma^2_{w^i} = p_i\sigma^2_s, \tag{11}$$

where $p^i = (D^TD)^{ii-1}$ is the i'th noise propagation coefficient associated with the modal IM D,[36] and σ^2_s is the normalized slope noise variance:

$$\sigma^2_s = \sum_k \left(\frac{\partial s}{\partial I_k}\right)^2 \sigma^2_{I^k} = \frac{\sum_k (x^k)^2\sigma^2_{I^k}}{\left(\sum_j I^j\right)^2}, \tag{12}$$

where the slope s is defined as

$$s = \frac{\sum_j x^j I^j}{\sum_j I^j}. \tag{13}$$

Here x are the quad-cell weights, I is the pixel intensity value, and σ^2_I is the pixel intensity value variance:

$$\sigma^2_{I^j} = F^2(n^j + b + d) + \sigma^2_e, \tag{14}$$

where n^j is the number of detected photons per frame for the j'th pixel, b is the number of detected photons from the sky background per frame per pixel, d is the dark current in electrons per frame per pixel, F is the excess noise factor (to be accounted if the detector is an electron multiplying charge-coupled device), and σ_e is the number of electrons root mean square (RMS) of readout noise per pixel. The p^i values have been obtained from the IM computed in end-to-end simulation in diffraction-limited conditions.

2.2.4 *Aliasing error*

For aliasing error we denote the spatial aliasing error made by the system WFS when it measures the residual WF incoming on the telescope pupil. The modal representation of this error is given as

$$\sigma^2_{\text{noise}} = \sum_i \int |H^i_n(\omega)|^2\text{PSD}\{a^i_{\text{alias}}\}\text{d}\omega, \tag{15}$$

where $H^i_n(\omega)$ is the NTF and a^i_{alias} is the input aliasing. In theory the aliasing term is given as

$$a^i_{\text{alias}}(n) = [R\mathbf{s}_{\text{turb}\perp}(n)]^i, \tag{16}$$

where $\mathbf{s}_{\text{turb}\perp}(n)$ represents the WFS measurement vector produced by all high-order modes at iteration n and R is the reconstruction matrix $R = D^\dagger$. The input to the system at each iteration consists in the high-order component of the

atmospheric phase, $\phi_{\text{turb}\perp}(n)$, responsible for the spatial aliasing error. The measurement of the WFS will give us an estimate of a_{alias}.

We chose to evaluate numerically the aliasing error using precorrected phase screens and open-loop WF sensing, because we want to take into account the temporal aspect that analytical formulas, such as the one described in Vérinaud,[37] do not model.

3 How to Use the Machine: Design and Optimization

For a given configuration of the AO system, the machine provides the estimation of the WF residuals with the breakdown in its components [see Eq. (6)]. The computation time for a single configuration with hundreds of degree of freedoms is about 2 orders of magnitude less than end-to-end simulations. This allows to explore a wide range in the parameter space. Moreover, the feedback on the error term distribution allows driving the parameter tuning to the best balance. This tool is extremely efficient for both AO system design and tuning as function of reference star brightness and seeing conditions.

We used the machine for the design and optimization of the SOUL[22] system and we report here this as real use case. SOUL is the LBT first light adaptive optics [first light adaptive optics (FLAO)][38] upgrade: a SCAO system with a 40×40 subaperture P-WFS and an ASM with 672 actuators.[39]

During the design phase, we used the machine for the trade-off study on the new WFS detector, where readout noise and readout time were two of the key points for the selection.

Table 1 Summary of the parameters to be explored in the optimization.

Parameter	Range	Unit
Sampling frequency	[50, 1500]	Hz
Modulation amplitude (radius)	[2, 6]	λ/D
Pupil sampling (side)	{10, 13.3, 20, 40}	Subaperture
No. of corrected modes	[5, 660]	—
Gain	[0.1, 2.0]	—

Then, once the system was designed, the machine has been extensively employed for the tuning of the system parameters under different conditions. The set of parameters explored are shown in Table 1 and the conditions considered are three seeing values, 0.6, 0.8. and 1.0 arc sec, a typical FLAO tip/tilt vibration spectrum (see Kulcsár et al.[40]) and reference star magnitudes between $R = 7.5$ and 17.5.

So, for a given condition that is a combination of seeing, vibration spectrum, and reference star magnitude, the optimization has been done computing the total error for each combination of the parameters defined in Table 1 and choosing the one with the smallest error. This computation requires few inputs that had been determined for all parameter configurations requested into the optimization before running the optimization itself:

- Reconstruction matrices (function of pupil sampling and modulation amplitude).
- Input aliasing (function pupil sampling). Examples of aliasing modal RMS and PSDs are shown in Fig. 2.
- WFS sensitivity loss factors ρ^i (function sampling and turbulence residual). For this parameter seven levels of total residual for each pupil sampling have been taken into account.[25] Information about these factors is reported in Sec. 2.1 and an example of them is shown in Fig. 3.

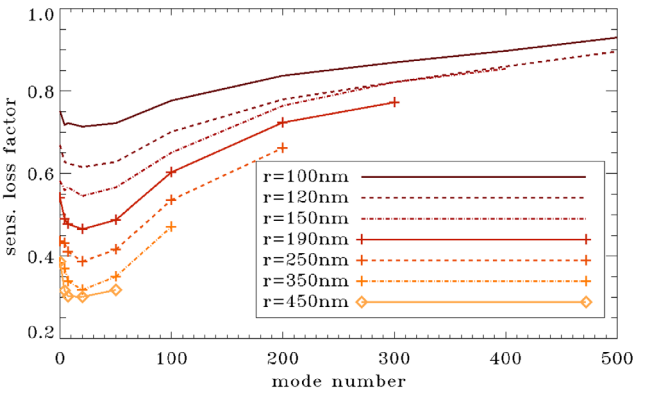

Fig. 3 WFS sensitivity loss factor ρ^i for different levels of residual r for 40×40 subaperture case. Note that levels of residual larger than 150 nm correspond to fewer corrected modes (<660) and, so, to larger fitting errors.

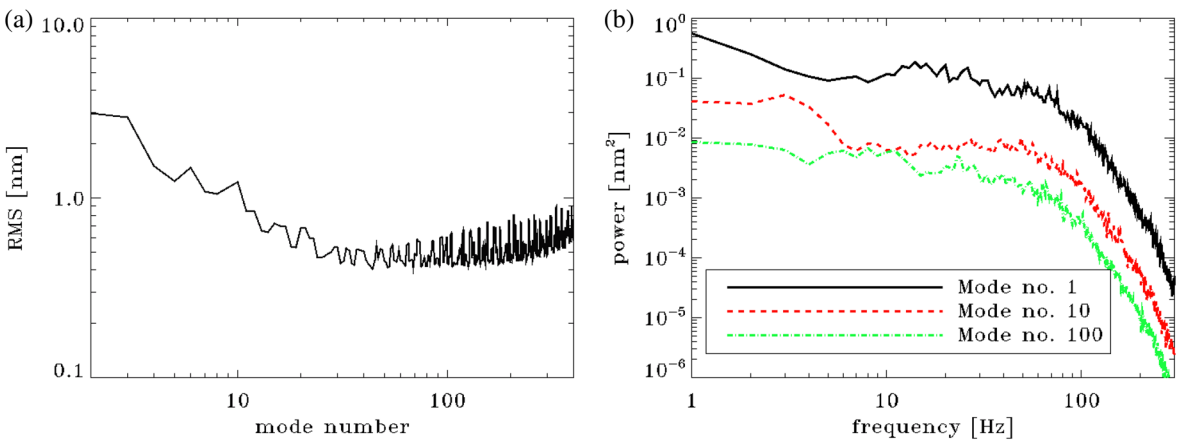

Fig. 2 Aliasing for 40 subaperture pupil sampling case: (a) modal RMS in nanometers and (b) PSDs for few modes. PSDs show that, differently than noise, aliasing is not white, and has a behavior similar to turbulence: almost flat for low frequencies and with a $f^{-17/3}$ asymptote on high frequencies.

In particular, the WFS sensitivity loss factor is chosen with an initial guess on the final total residual [Eq. (6)]. An iterative procedure can improve the initial guess, but it has not been implemented in this work. Note that, during the optimization, CLTF stability is checked before computing the total error, because some combinations of parameters (sampling frequency and integrator gain) can give an unstable system. These unstable cases are discarded. We chose to optimize a gain equal for each mode with the exception of tip/tilt when a telescope structure vibration is considered, but a modal control optimization[41] can be done, optimizing one mode at a time, and more complex control filters can be considered.

The results of the optimization are reported in three tables: Tables 2 and 3 show results with seeing 0.8 arc sec and with and without tip/tilt telescope structure vibrations, respectively, and, in Table 4, results with different seeing values are presented. Moreover, the relative contributions of the error terms, for the case of Tables 2 and 3 results, are shown in Fig. 4. The optimization, as expected, gives high temporal and spatial sampling for bright stars ($R \leq 10.5$). Here, the budget is dominated by

Table 2 Summary of error budget optimization for SOUL with different reference star magnitude values, seeing 0.8 arc sec.

Mag. *R*	SR (H) (%)	Tot. (nm)	Fitt. (nm)	Time (nm)	Noise (nm)	Alias. (nm)	# s.a.	Fr. (Hz)	Flux (ph/fr)	# Modes	Gain
7.5	90.3	84.0	73.1	31.7	14.1	22.4	40	1500	196,187	660	0.50
8.5	89.9	85.6	73.1	31.0	22.4	22.5	40	1500	78,123	660	0.50
9.5	89.2	88.8	73.1	37.5	28.6	17.8	40	1500	31,149	660	0.40
10.5	87.5	96.0	73.1	43.4	41.7	15.7	40	1500	12,434	660	0.35
11.5	83.4	112.0	74.7	57.4	56.0	23.1	40	500	14,821	633	0.90
12.5	77.1	133.9	85.3	69.2	73.8	20.6	40	400	7410	471	1.00
13.5	65.7	170.3	102.7	84.2	105.0	18.1	40	300	3894	312	1.20
14.5	50.2	218.1	127.8	104.9	138.8	31.5	20	300	1570	192	0.90
15.5	29.5	290.3	179.7	143.1	170.7	48.7	13.3	200	921	90	1.00
16.5	13.1	374.5	226.1	194.4	220.6	51.4	10	200	367	54	0.70
17.5	4.4	463.4	226.1	272.0	294.4	54.2	10	100	291	54	0.90

Note: Mag., star magnitude; Tot., total error; Fitt., fitting error; Alias., aliasing error; Fr., frequency; s.a., subaperture.

Table 3 Summary of error budget optimization for SOUL with different reference star magnitude values, seeing 0.8 arc sec and considering telescope structure vibrations.

Mag. *R*	SR (H) (%)	Tot. (nm)	Fitt. (nm)	Time (nm)	Noise (nm)	Alias. (nm)	# s.a.	Fr. (Hz)	Flux (ph/fr)	# Modes	High Orders Gain	Tip/Tilt Gain
7.5	84.5	107.6	73.1	71.7	21.8	24.7	40	1500	196,187	660	0.50	0.95
8.5	83.9	110.2	73.1	74.4	28.4	21.6	40	1500	78,123	660	0.45	0.90
9.5	82.3	115.9	73.1	76.1	43.8	19.5	40	1500	32,404	660	0.40	0.90
10.5	78.6	128.8	73.1	88.5	55.9	16.7	40	1500	12,434	660	0.35	0.90
11.5	71.1	153.5	76.3	104.2	81.8	13.9	40	1500	4898	603	0.30	0.90
12.5	57.6	195.1	90.8	121.4	122.4	11.9	40	1400	2135	410	0.30	0.90
13.5	40.5	249.7	123.0	141.8	163.0	24.2	20	1200	977	209	0.30	0.80
14.5	21.1	327.8	180.0	195.9	186.8	44.0	13.3	600	782	90	0.50	1.30
15.5	8.5	412.3	226.1	250.7	231.7	48.6	10	500	369	54	0.40	1.20
16.5	2.2	512.9	226.1	319.6	327.7	49.4	10	300	243	54	0.50	1.50
17.5	0.1	684.2	226.1	451.6	459.1	47.8	10	200	149	54	0.50	1.40

Note: Mag., star magnitude; Tot., total error; Fitt., fitting error; Alias., aliasing error; Fr., frequency; s.a., subaperture.

Table 4 Summary of error budget optimization for SOUL with different seeing and reference star magnitude values.

Seeing (arc sec)	Mag. *R*	SR (H) (%)	Tot. (nm)	Fitt. (nm)	Time (nm)	Noise (nm)	Alias. (nm)	# s.a.	Fr. (Hz)	Flux (ph/fr)	# Modes	Gain
0.6	8.5	93.2	69.6	57.6	27.1	20.0	20.0	40	1500	78,123	660	0.45
0.8	8.5	89.9	85.6	73.1	31.0	22.4	22.5	40	1500	78,123	660	0.50
1.0	8.5	86.3	100.8	88.1	37.4	22.4	22.5	40	1500	78,123	660	0.50
0.6	12.5	82.7	114.5	69.7	59.9	65.8	18.3	40	400	7410	430	0.90
0.8	12.5	77.1	133.9	85.3	69.2	73.8	20.6	40	400	7410	470	1.00
1.0	12.5	71.7	151.6	97.8	76.5	83.8	23.5	40	400	7410	530	1.10
0.6	16.5	21.7	324.8	177.9	175.3	202.2	47.1	10	200	369	54	0.60
0.8	16.5	13.1	374.5	226.1	194.4	220.6	51.4	10	200	369	54	0.70
1.0	16.5	7.7	420.8	272.3	207.6	238.2	55.5	10	200	369	54	0.80

Note: Mag., star magnitude; Tot., total error; Fitt., fitting error; Alias., aliasing error; Fr., frequency; s.a., subaperture.

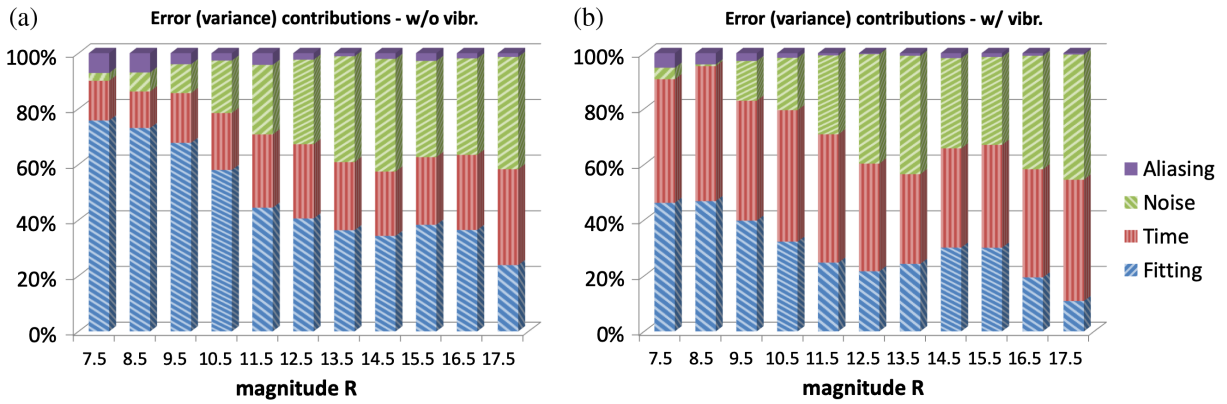

Fig. 4 The residual WF variance components allocation estimated by the error budget at seeing 0.8″ and (a) without and (b) with vibrations.

the fitting error due to the limited number of actuators on the DM. Then, going to fainter magnitudes, the temporal and spatial sampling is gradually reduced. The way they are reduced greatly depends on the telescope structure vibrations: in fact, when they are present, the optimization reduces the spatial sampling faster in order to keep high temporal frequency to minimize the temporal error, which dominates the budget. Instead, without vibrations, the spatial sampling is maintained on high levels to minimize the fitting error, which, in this case, is the largest term. From $R = 11.5$, the number of actuators is no longer the limiting factor and, as expected, the machine sets the parameters equalizing noise, time, and fitting errors. Finally, when the seeing increases, the optimization does not change the spatial and temporal sampling but selects a higher integrator gain, and, for $R = 12.5$, a larger number of modes. This is done in order to decrease the temporal and, for $R = 12.5$, fitting errors with relatively low impact on other error terms.

4 Cross Check with Numerical Simulations

In this section we will demonstrate that the machine described in this work is reliable and effective by means of a comparison with end-to-end simulation results. We performed end-to-end simulations with PASSATA[42] using the same sampling frequency, modulation amplitude, and pupil sampling of the error budget machine. We reoptimized the number of corrected modes and integrator gains and found few discrepancies on integrator gains. These discrepancies are limited to high-magnitude cases where performance is poor. In this condition, our initial guess of total residual, and so the WFS sensitivity loss factor (see Sec. 3), is less accurate. Hence, the iterative procedure to estimate this factor proposed in the previous section can improve the results.

The comparison with end-to-end simulations is shown in Fig. 5; we can conclude that the results obtained by the two methods are in good agreement, and the small differences should be mainly related to the limited accuracy in the choice of the WFS sensitivity loss factor.

5 Conclusions

In this work, we have presented an error budget software for AO systems with P-WFS. This software uses a semianalytical approach with numerical models and computes accurate estimates of the response of a nonlinear WFS, such as the P-WFS. This gives us a powerful tool, which is complementary to

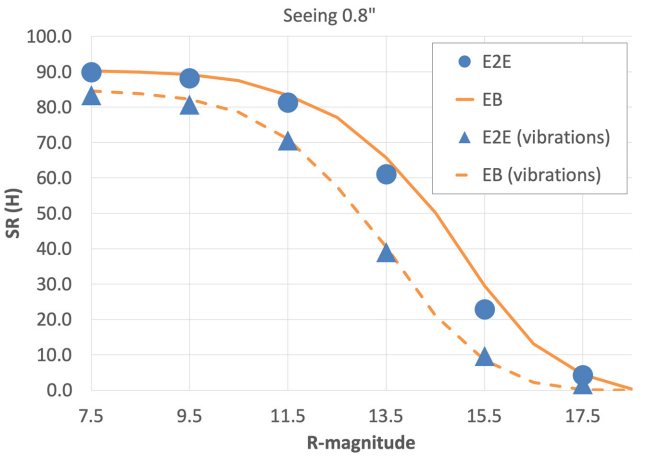

Fig. 5 Comparison between PASSATA end-to-end simulations (E2E label) and error budget (EB label) results. SR (H band) in function of the guide star R-magnitude.

end-to-end simulations and perfect to explore huge range of system parameters both in design and optimization phases. The case of the SOUL system shows a real case of application where the error budget software demonstrated its potential, providing the optimization of the AO parameters and the estimation for each component of the residual WF. The comparison with end-to-end simulations demonstrates the reliability of the error budget output with an accuracy of few percentage of SR in the complete range of explored reference star magnitudes.

Finally, given the recent availability of an analytical model for the P-WFS in partial correction,[20] the natural evolution of the presented work is the implementation of such model moving toward a full analytical tool for AO system with P-WFS.

We believe that this kind of software can be a key tool in the development and tuning of the next generation of AO systems with P-WFS, such as the SCAO for the 25- to 40-m class of telescopes, where end-to-end simulations become more and more expensive in terms of computational time.

References

1. J. M. Hill, "The large binocular telescope," *Appl. Opt.* **49**, D115–D122 (2010).
2. R. Arsenault et al., "ESO adaptive optics facility progress report," *Proc. SPIE* **8447**, 84470J (2012).
3. K. M. Morzinski et al., "MagAO: status and science," *Proc. SPIE* **9909**, 990901 (2016).
4. B. Neichel et al., "Gemini multiconjugate adaptive optics system review—II. Commissioning, operation and overall performance," *MNRAS* **440**, 1002–1019 (2014).
5. S. M. Adkins et al., "New developments in instrumentation at the W. M. Keck Observatory," *Proc. SPIE* **9908**, 990805 (2016).
6. A. H. Bouchez et al., "An overview and status of GMT active and adaptive optics," *Proc. SPIE* **10703**, 107030W (2016).
7. E. Pinna et al., "Design and numerical simulations of the GMT natural guide star WFS," *Proc. SPIE* **9148**, 91482M (2014).
8. M. Wang et al., "Optical designs of the LGS WFS system for GMT-LTAO," *Proc. SPIE* **8447**, 84473Q (2012).
9. P. M. Hinz et al., "Design and predicted performance of the GMT ground-layer adaptive optics mode," *Proc. SPIE* **8447**, 84473R (2012).
10. E. Diolaiti et al., "MAORY: adaptive optics module for the E-ELT," *Proc. SPIE* **9909**, 99092D (2016).
11. B. Neichel et al., "The adaptive optics modes for HARMONI: from classical to laser assisted tomographic AO," *Proc. SPIE* **9909**, 990909 (2016).
12. G. Herriot et al., "NFIRAOS: first facility AO system for the Thirty Meter Telescope," *Proc. SPIE* **9148**, 914810 (2014).
13. F. J. Rigaut, J.-P. Veran, and O. Lai, "Analytical model for Shack–Hartmann-based adaptive optics systems," *Proc. SPIE* **3353**, 1038–1048 (1998).
14. L. Jolissaint, J.-P. Véran, and R. Conan, "Analytical modeling of adaptive optics: foundations of the phase spatial power spectrum approach," *J. Opt. Soc. Am. A* **23**, 382–394 (2006).
15. L. Jolissaint, "Synthetic modeling of astronomical closed loop adaptive optics," *J. Eur. Opt. Soc.* **5**, 10055 (2010).
16. B. L. Ellerbroek, "Linear systems modeling of adaptive optics in the spatial-frequency domain," *J. Opt. Soc. Am. A* **22**, 310–322 (2005).
17. F. E. Zocchi, "A simple analytical model of adaptive optics for direct detection free-space optical communication," *Opt. Commun.* **248**, 359–374 (2005).
18. S. Thomas et al., "Comparison of centroid computation algorithms in a Shack–Hartmann sensor," *MNRAS* **371**, 323–336 (2006).
19. B. Neichel, T. Fusco, and J.-M. Conan, "Tomographic reconstruction for wide-field adaptive optics systems: Fourier domain analysis and fundamental limitations," *J. Opt. Soc. Am. A* **26**, 219–235 (2009).
20. O. Fauvarque et al., "Kernel formalism applied to Fourier-based wavefront sensing in presence of residual phases," *J. Opt. Soc. Am. A* **36**, 1241 (2019).
21. S. Esposito and A. Riccardi, "Pyramid wavefront sensor behavior in partial correction adaptive optic systems," *Astron. Astrophys.* **369**, L9–L12 (2001).
22. E. Pinna et al., "SOUL: the single conjugated adaptive optics upgrade for LBT," *Proc. SPIE* **9909**, 99093V (2016).
23. T. Fusco et al., "High-order adaptive optics requirements for direct detection of extrasolar planets: application to the SPHERE instrument," *Opt. Express* **14**, 7515–7534 (2006).
24. J. M. Beckers, "Adaptive optics for astronomy—Principles, performance, and applications," *Annu. Rev. Astron. Astrophys.* **31**, 13–62 (1993).
25. G. Agapito et al., "Elephants, goldfishes and SOUL: a dissertation on forgetfulness and control systems," in *Adapt. Opt. for Extremely Large Telesc. 6—Conf. Proc.* (2019).
26. J. Y. Wang and J. K. Markey, "Modal compensation of atmospheric turbulence phase distortion," *J. Opt. Soc. Am.* **68**, 78–87 (1978).
27. V. Korkiakoski, C. Vérinaud, and M. L. Louarn, "Improving the performance of a pyramid wavefront sensor with modal sensitivity compensation," *Appl. Opt.* **47**, 79–87 (2008).
28. S. Esposito et al., "Non common path aberration correction with non linear WFSs," in *Adapt. Opt. for Extremely Large Telesc. 4—Conf. Proc.* (2002).
29. G. Agapito, C. Arcidiacono, and S. Esposito, "Shack–Hartmann wavefront sensor sensitivity loss factor estimation in partial correction regime," in *Proc. fifth Adapt. Opt. for Extremely Large Telesc. Conf.* (2017).
30. V. Deo et al., "A modal approach to optical gain compensation for the pyramid wavefront sensor," *Proc. SPIE* **10703**, 1070320 (2018).
31. D. L. Fried, "Anisoplanatism in adaptive optics," *J. Opt. Soc. Am.* **72**, 52–61 (1982).
32. F. Roddier, *Adaptive Optics in Astronomy*, Cambridge University Press, Cambridge (1999).
33. M. Born and E. Wolf, *Principles of Optics Electromagnetic Theory of Propagation, Interference and Diffraction of Light*, Cambridge University Press, Cambridge (1980).
34. F. Quirós-Pacheco et al., "First light AO (FLAO) system for LBT: performance analysis and optimization," *Proc. SPIE* **7736**, 77363H (2010).
35. J. M. Conan, G. Rousset, and P. Y. Madec, "Wave-front temporal spectra in high-resolution imaging through turbulence," *J. Opt. Soc. Am. A* **12**(7), 1559–1570 (1995).
36. F. Rigaut and E. Gendron, "Laser guide star in adaptive optics—the tilt determination problem," *Astron. Astrophys.* **261**, 677–684 (1992).
37. C. Vérinaud, "On the nature of the measurements provided by a pyramid wave-front sensor," *Opt. Commun.* **233**, 27–38 (2004).
38. S. Esposito et al., "First light AO (FLAO) system for LBT: final integration, acceptance test in Europe, and preliminary on-sky commissioning results," *Proc. SPIE* **7736**, 773609 (2010).

39. A. Riccardi et al., "The adaptive secondary mirror for the large binocular telescope: results of acceptance laboratory test," *Proc. SPIE* **7015**, 701512 (2008).
40. C. Kulcsár et al., "Vibrations in AO control: a short analysis of on-sky data around the world," *Proc. SPIE* **8447**, 84471C (2012).
41. E. Gendron and P. Lena, "Astronomical adaptive optics. 1. Modal control optimization," *Astron. Astrophys.* **291**(1), 337–347 (1994).
42. G. Agapito, A. Puglisi, and S. Esposito, "PASSATA: object oriented numerical simulation software for adaptive optics," *Proc. SPIE* **9909**, 99097E (2016).

Guido Agapito is a researcher at INAF, Osservatorio Astrofisico di Arcetri, Adaptive Optics Group. He has 10 years of experience in adaptive optics for astronomy, and he is currently involved in several projects, including Multiconjugate Adaptive Optics RelaY (MAORY) for ELT, Enhanced Resolution Imager and Spectrograph (ERIS), and First Light Adaptive Optics (FLAO) system. He is an expert of AO control systems, and he is the main developer of the Pyramid Simulator Software for Adaptive Optics Arcetri (PASSATA).

Enrico Pinna: Biography is not available.